

**Nitrogen adsorption on carbon nanotube bundles: Role of the external surface**

Jianwen Jiang\* and Stanley I. Sandler

*Center for Molecular and Engineering Thermodynamics, Department of Chemical Engineering, University of Delaware, Newark, Delaware 19716, USA*

(Received 6 July 2003; published 12 December 2003)

Nitrogen adsorption on two types of single-walled carbon nanotube bundles at both subcritical and supercritical temperatures is studied using Gibbs ensemble Monte Carlo simulation to understand the role of the external surface in the type of isotherm. On an infinite periodic hexagonal bundle *without* an external surface, which was mostly used in previous theoretical studies, subcritical adsorption is of type I with two steps in the adsorption isotherm and two maxima in the isosteric heat corresponding to adsorption, first forming annuli inside the nanotubes, and then with increased coverage at the centers of the nanotubes. Supercritical adsorption is also of type I, but with one step in the adsorption isotherm and a single maximum in the isosteric heat. Also, at high pressures the interstitial channels between the nanotubes become accessible to nitrogen molecules. On a small isolated hexagonal bundle *with* an external surface, subcritical adsorption is of type II, as has been observed in experiments, with two steps in the adsorption isotherm and two maxima in the isosteric heat. The first step corresponds to adsorption at the internal annuli and the grooves between the nanotubes, and the second step results from adsorption at the ridges on the external surface of the bundle and at the centers of the nanotubes. At higher coverages multilayer adsorption and wetting occur on the external surface as the bulk phase approaches saturation. Supercritical adsorption is of type I, without a step in the adsorption isotherm or a maximum in the isosteric heat, and there is no nitrogen adsorption in the interstitial channels even at high pressures. These results demonstrate the important role of the external surface of the nanotube bundle in the character of adsorption isotherm, and provide a substantial physical explanation for the difference between experimental observation and previous theoretical prediction.

DOI: 10.1103/PhysRevB.68.245412

PACS number(s): 68.43.-h, 81.05.Rm, 05.70.-a

**I. INTRODUCTION**

Since their discovery by Iijima in 1991,<sup>1</sup> carbon nanotubes have stimulated intense interest in physics, chemistry, material science, and biology.<sup>2</sup> Carbon nanotubes have a variety of superior properties including well-defined nanodimensional structure, high electrical and thermal conductivity, good mechanical stability, etc.<sup>3,4</sup> These structures provide a large specific surface area per unit weight, indeed, higher than that of graphite, although the density is lower due to the hollow interiors. This suggests that carbon nanotubes could be excellent candidates for gas storage, purification, and separation.

There have been a large number of experimental investigations of gas adsorption on carbon nanotubes. For example, the adsorption isotherms of nitrogen,<sup>5</sup> oxygen,<sup>5</sup> methane,<sup>6</sup> and krypton<sup>6</sup> on single-walled carbon nanotube (SWNT) bundles were measured near 77 K, and all found to be type II according to the IUPAC (International Union of Pure and Applied Chemistry) classification. A similar isotherm was reported for nitrogen adsorption at 71 K on closed-ended SWNT bundles,<sup>7</sup> and it was found that the adsorption of nitrogen on open-ended SWNT bundles is three times larger than on closed-ended SWNT bundles.<sup>8</sup> Nitrogen,<sup>9</sup> methane,<sup>10</sup> and butane<sup>11</sup> adsorption isotherms on multiwalled carbon nanotubes (MWNT) bundles have also been found to be type II. Much work has been done on hydrogen adsorption on carbon nanotubes at both cryogenic and ambient temperatures toward developing renewable and environmentally friendly pollution-free fuel cell technology for future electric vehicles; for details, see recent reviews.<sup>12-16</sup>

Molecular simulations, first-principles quantum mechanics methods, and their combinations, have been applied to aim to understand gas adsorption on nanotube bundles. Studies of gas adsorption inside a single SWNT or MWNT are not mentioned here, as that is not the focus of this work. Simulations have been conducted on SWNT square bundles for the physisorption of nitrogen at 77 K;<sup>17</sup> of methane at 75, 148, and 300 K;<sup>18</sup> of ethane at 180 K;<sup>19</sup> and of hydrogen at 77 K,<sup>20,21</sup> 293 K,<sup>22-24</sup> and 298 K.<sup>20</sup> Also there have been simulations on SWNT hexagonal bundles for the physisorption of hydrogen at 77 K,<sup>20,21,25</sup> 293 K,<sup>23,25</sup> and 298 K,<sup>20,26,27</sup> of xenon at 95 K,<sup>28</sup> and of hydrogen on heterogeneous SWNT bundles at 298 K.<sup>29</sup> To take into account quantum effects of light gas molecules at very low temperatures or to investigate gas chemisorption on SWNT bundles, quantum mechanics methods have been employed, including path integral simulation,<sup>30</sup> *ab initio* simulation,<sup>31</sup> and density functional theory.<sup>32</sup>

The adsorption isotherms that have been predicted theoretically are of type I, or in a few cases type IV, independent of temperature. Physically, the prediction of a type I isotherm is not unexpected at bulk adsorbate supercritical temperatures as multilayer adsorption is not likely to occur. However, at subcritical temperatures, where multiple adsorption layers may form and wetting may occur, the theoretical prediction is not in agreement with the experimental observation of type II isotherms. This difference is, as shown here, the result that an infinite periodic nanotube bundle *without* an external surface was assumed theoretically. However, experiments<sup>5,33,34</sup> have shown that nanotubes form hexagonal bundles that are nearly uniform and of finite diameter. Con-

TABLE I. Parameters  $c_k$  in the endohedral and exohedral averaged potentials of a nitrogen atom along the radial distance from the center of a (10,10) SWNT.

$k$	0	1	2	3	4	5	6	7	8
Endohedral	9276.09	-49227.1	105086	-121229	83007.9	-34674.7	8608.90	-1173.05	72.31
Exohedral	5.797	66.41	314.03	799.83	1185.09	1150.62	651.71	210.08	30.73

sequently, the external surface of a finite bundle ought to be available for gas adsorption, and experimental evidence for this has been provided by gas adsorption on closed-ended SWNT bundles.<sup>35-38</sup> Only recently have there been a few simulations examining the effect of the external surface on gas adsorption on SWNT bundles for hydrogen at supercritical temperatures,<sup>39</sup> and for a variety of gases (neon, argon, krypton, xenon, and methane) at subcritical temperatures.<sup>40-42</sup> In the latter, the adsorption isotherms were found to be type II, consistent with experimental observation. This suggests that to correctly predict adsorption on the nanotube bundles, the external surface must be taken into account.

The goal of this work is to more thoroughly explore the role of the external surface in gas physisorption at both subcritical and supercritical temperatures on two types of SWNT bundles: an infinite periodic hexagonal bundle that does not have an external surface, and a finite isolated hexagonal bundle that does have an external surface. Open-ended SWNTs are considered here to allow gas endohedral adsorption inside the nanotubes in addition to exohedral adsorption on the external surface, which is different from earlier studies,<sup>40-42</sup> in which adsorption only on the external surface at subcritical temperatures was considered.

In Sec. II the atomistic models of the two types of SWNT bundles under study are described in detail and the favorable adsorption sites are identified, followed in Sec. III by a discussion of simulation methods. In Sec. IV, the simulated density distributions of adsorbed nitrogen molecules, the locations of their centers of mass, the adsorption isotherms, and the isosteric heats are presented on both types of bundles at two subcritical temperatures, 77 and 100 K, and one supercritical temperature, 300 K. Finally, concluding remarks are given in Sec. V. Note that the critical temperature of nitrogen is about 126 K.<sup>43</sup> Traditionally, one uses the term “gas adsorption” to refer to the adsorption at supercritical temperatures, and “vapor adsorption” at subcritical temperatures. Throughout this manuscript, we simply use “gas adsorption” to refer to both cases.

## II. MODELS

A SWNT is a seamless cylinder formed by rolling up a graphene sheet. The SWNT under study is the metallic armchair type with a highly symmetrical structure, a Hamada index of (10,10), and a diameter of 13.56 Å, as this SWNT is the most frequently observed experimentally.<sup>33</sup> The armchair SWNT is comprised of cylindrical sheet of hexagons with long axes perpendicular to the tube axis, while they are parallel in the zigzag SWNT. The adsorbate, nitrogen, is represented by a rigid two-site molecule with a fixed bond length

of 1.10 Å, unlike other simulation studies of nitrogen adsorption in nanotubes,<sup>17</sup> in which nitrogen had been represented by a spherical molecule. Such an assumption is probably not appropriate as the molecular dimensions of the adsorbate and the nanotube diameter are of the same order of magnitude. The nitrogen-nitrogen interaction is modeled by the Lennard-Jones potential with a well depth  $\epsilon_{N-N}/k_B = 36.4$  K ( $k_B$  is the Boltzmann constant) and a collision diameter  $\sigma_{N-N} = 3.32$  Å, which were fitted to the experimental bulk properties of nitrogen.<sup>44</sup> It has been found that the nanotube-xenon interaction can be approximated by the graphite-xenon interaction since a nanotube can be considered as a rolled up graphene sheet.<sup>28</sup> Similarly, to model the nanotube-nitrogen interaction, we use the Lennard-Jones potential with parameters  $\epsilon_{C-N}/k_B = 33.4$  K and  $\sigma_{C-N} = 3.36$  Å, which were fitted to the measured properties of nitrogen adsorption on graphite in the limit of zero coverage.<sup>45</sup>

The open-ended nanotube is considered to be infinitely long along the tube axis; consequently, averaging over the tube axis leads to a nanotube-nitrogen potential that depends only on the radial distance  $r$  from the tube center. We first calculate the explicit potential for a nitrogen atom at a given radial distance  $r$  by accounting for the frozen carbon atoms explicitly, and then fit the results to a polynomial function of  $r$  of the form

$$u(r) = \sum_{k=0}^8 c_k \left( \frac{R}{R-r} \right)^k, \quad (1)$$

where  $R = 6.78$  Å is the radius of the (10,10) nanotube. The endohedral (inside) and exohedral (outside) averaged potentials are fitted separately and the parameters  $c_k$  are given in Table I. Using these averaged potentials, simulations are significantly accelerated without a significant loss of accuracy.

Because of the van der Waals interactions, nanotubes form hexagonal bundles of finite diameter. The average number of nanotubes within a bundle varies with the synthesis method. For example, bundles between 100 and 500,<sup>33</sup> and of the order of 20 nanotubes<sup>34</sup> have been reported. For (10,10) SWNT bundles the experimentally measured intertube distance, i.e., the van der Waals gap, is nearly constant at 3.2 Å.<sup>33,34</sup> Although there have been a few simulation studies on gas adsorption in square bundles,<sup>18,24</sup> the formation of hexagonal bundles is energetically more favorable. Such hexagonal bundles have also been found in some polymeric supramolecules formed by self-assembly.<sup>46</sup>

To investigate the effect of the external surface of a SWNT bundle on gas adsorption, we compare nitrogen adsorption in two types of (10,10) SWNT bundles: (i) an infinite periodic hexagonal bundle *without* an external surface, and (ii) a finite isolated hexagonal bundle *with* an external

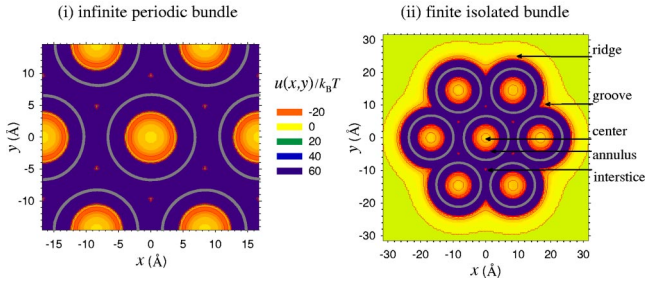


FIG. 1. (Color online) Potential energy  $u(x,y)/k_B T$  ( $T=77$  K) contours in the  $x$ - $y$  plane for a nitrogen molecule aligned parallel to the tube axis in the  $z$  dimension on (i) the infinite periodic bundle and (ii) the finite isolated bundle. The favorable adsorption sites are indicated in (ii).

surface. A periodic rectangular parallelepiped of  $33.5 \text{ \AA} \times 29.0 \text{ \AA} \times 36.9 \text{ \AA}$  with aligned hexagonal (10,10) SWNTs is used to represent the infinite periodic bundle. This is shown in Fig. 1(i) where the large circles are the SWNT walls with the tube axis in the  $z$  dimension. The finite isolated bundle is assumed to be composed of seven (10,10) SWNTs with a diameter of approximately  $47 \text{ \AA}$  in a periodic rectangular parallelepiped of  $100.0 \text{ \AA} \times 100.0 \text{ \AA} \times 36.9 \text{ \AA}$ . The lengths in the  $x$  and  $y$  dimensions are sufficiently large to eliminate the nearest neighbor interactions with its periodic images, to ensure that the bundle is truly isolated. Shown in Fig. 1(ii) is the central region of the finite isolated bundle.

To identify the likely favorable adsorption sites, Fig. 1 further shows the potential energy  $u(x,y)/k_B T$  ( $T=77$  K) contours in the  $x$ - $y$  plane of a nitrogen molecule kept parallel to the nanotube axis in (i) the infinite periodic bundle and (ii) the finite isolated bundle. The energy is calculated between a nitrogen molecule parallel to the tube axis at a given position with all the carbon atoms in the bundle. The favorable adsorption sites are indicated in (ii) with the corresponding potential energies given in Table II. For the periodic bundle without an external surface, all the nanotubes are identical, and there are no groove and ridge sites. The most favorable site is the annulus at  $3.4 \text{ \AA}$  from the nanotube center with

TABLE II. Potential energy  $u(x,y)/k_B T$  ( $T=77$  K) at the favorable adsorption sites for a nitrogen molecule aligned parallel to the nanotube axis.

Adsorption site	(i) Periodic bundle	(ii) Isolated bundle
Annulus	-23.0	-22.8 <sup>a</sup>
Center	-7.8	-7.6 <sup>b</sup>
Interstice	-4.4	-4.4
Groove	c	-23.0
Ridge	c	-11.4

<sup>a</sup>-22.8 inside the middle nanotube and inhomogeneous inside the neighboring nanotubes.

<sup>b</sup>-7.6 inside the middle nanotube and -7.2 inside the neighboring nanotubes.

<sup>c</sup>Due to the periodic geometry, there are no groove and ridge sites on the periodic bundle.

$u/k_B T = -23.0$ , and a somewhat less favorable site is the nanotube center with  $u/k_B T = -7.8$ . The adsorption site at the interstice bounded by three nanotubes is a narrow channel at  $9.7 \text{ \AA}$  from the nanotube center with  $u/k_B T = -4.4$ , and the interstices surrounding each nanotube form a honeycomb lattice. For the isolated bundle, the most favorable site is the groove between two adjacent nanotubes with  $u/k_B T = -23.0$ , but this site is a very small region at  $20.2 \text{ \AA}$  from the bundle center. Another favorable site is the annulus at  $3.4 \text{ \AA}$  from the center of the middle nanotube with  $u/k_B T = -22.8$ . The interaction energy at the annulus inside the nanotube surrounding the middle nanotube is not uniform, and is more attractive closer to the middle. The next most favorable site is the ridge surrounding the nanotube on the external surface with  $u/k_B T = -11.4$ , then the center of the middle nanotube with  $u/k_B T = -7.6$ , and the center of the neighboring nanotube with  $u/k_B T = -7.2$ . Similar to the periodic bundle, the interstice here also has an energy of  $u/k_B T = -4.4$  at  $9.7 \text{ \AA}$  from the bundle center. In the region of the external surface starting from the ridge, the attractive energy decreases with increasing distance from the bundle. Sufficiently far from the bundle, bulk gas behavior is reached as the gas molecules do not interact with the nanotubes.

### III. METHODS

The grand canonical Monte Carlo (GCMC) simulation<sup>47</sup> with the chemical potential of adsorbate fixed is widely used to study gas adsorption. Usually adsorption is analyzed as a function of bulk pressure, so an accurate equation of state or simulation of the bulk phase is needed to convert the chemical potential to bulk pressure. However, an accurate equation of state may not be available *a priori*, and additional simulation may be time consuming, especially for a wide range of temperatures and pressures. Consequently, the bulk phase is usually assumed to be an ideal gas; however, this assumption fails at high pressures, such as those of interest here.

In this work we employ the isobaric isothermal Gibbs ensemble Monte Carlo (*NPT* GEMC) simulation. The GEMC simulation was initially proposed to simulate phase equilibria,<sup>48,49</sup> in which two simulation cells are used, one for the low-density phase and the other for the high-density phase. In such a simulation, the total number of molecules is fixed, but molecules can be transferred from one cell to the other. The volume of each simulation cell is allowed to fluctuate to maintain pressure equality between the two bulk phases. Two simulation cells are also used for adsorption, but one with adsorbent and the other with bulk fluid. The volume of the adsorbent is fixed, but that of the bulk phase can be either fixed<sup>50</sup> or permitted to change at fixed bulk pressure.<sup>51</sup>

The *NPT* GEMC simulation was previously adapted by us to investigate the adsorption of pure oxygen, pure nitrogen, and their mixtures on the  $C_{168}$  schwarzite structure, and results consistent with those of the GCMC simulation were obtained.<sup>52,53</sup> From the *NPT* GEMC simulation one obtains the extent of adsorption at fixed bulk pressure, as well as the bulk density and enthalpy. This information is useful in computing the isosteric heat of adsorption given by<sup>54</sup>

$$q_{st} = H_B - \left( \frac{\partial U_A}{\partial N_A} \right)_{T, V_A}, \quad (2)$$

where  $H_B$  is the bulk enthalpy,  $U_A$  is the adsorption energy, and  $N_A$  is the number of admolecules. The isosteric heat of adsorption is a quantity used to measure the change of interactions during adsorption. At conditions at which the bulk fluid is an ideal gas,  $H_B$  can be approximated by  $R_g T$  where  $R_g$  is the gas constant. As mentioned earlier, gas molecules far from the isolated bundle do not interact with the carbons, and the density approaches the bulk density. Consequently, the number of admolecules is the total number of gas molecules in the simulation cell with adsorbent as corrected by subtracting the number of gas molecules behaving as bulk gas. To do so, a cutoff distance from the center of the isolated bundle is selected, within which the gas molecules are considered adsorbed. Note that this correction is negligible at low pressures, but it is significant at high pressures.

Five types of trial moves are conducted randomly in the  $NPT$  GEMC simulation here, displacement, rotation, creation, and deletion in each phase, and volume change of the bulk phase. For the first two types of moves, the number of molecules in each phase is fixed and a randomly chosen molecule is moved. The acceptance probability is determined by the Metropolis criterion

$$\min[1, \exp(-\beta\Delta U)], \quad (3)$$

where  $\Delta U$  is the change of the total energy of a trial move, and  $\beta = 1/k_B T$ . Creation of a molecule in the adsorbed (A) phase, corresponding to deletion of that molecule in the bulk (B) phase, is accepted with a probability of

$$\min\{1, \exp[-\beta(\Delta U_A + \Delta U_B)] N_A V_B / (N_B + 1) V_A\}. \quad (4)$$

Similarly, the probability of acceptance for the deletion of a molecule in the A phase and its creation in the B phase is

$$\min\{1, \exp[-\beta(\Delta U_A + \Delta U_B)] N_B V_A / (N_A + 1) V_B\}. \quad (5)$$

The acceptance probability for the trial volume change in the bulk phase is

$$\min\{1, \exp[-\beta\Delta U_B - \beta P \Delta V_B + N_B \ln(1 + \Delta V_B / V_B)]\}. \quad (6)$$

The cutoff length used for the calculation of the Lennard-Jones site-site interaction is 14.5 Å in the periodic bundle and 18.4 Å in the isolated bundle. There is no significant change in the simulation results by increasing the cutoff length, and thus no long-range correction is applied. Periodic boundary conditions are implemented in all three dimensions. Typical simulations consist of  $2 \times 10^4$  cycles and 5000 trial moves per cycle, with the first  $10^4$  cycles used for equilibration, and the second  $10^4$  cycles used to determine ensemble averages. At low temperatures or high coverages, additional trial moves are required to obtain precise averages. The block transformation method has been used to estimate the statistical error.<sup>55</sup> For example, nitrogen adsorp-

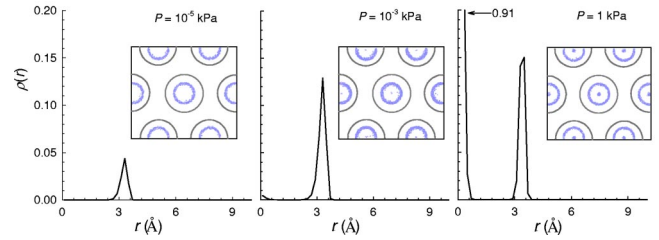


FIG. 2. (Color online) Density profiles of the centers of mass of nitrogen molecules versus the distance from the center of the periodic bundle at 77 K. The insets are snapshots generated by accumulating 50 equilibrium configurations.

tion on the periodic bundle at 77 K and 10 kPa expressed as the ratio of the number of nitrogen molecules to the number of carbon atoms is  $N_2/C = 0.10$ , which has a standard deviation of  $1.7 \times 10^{-4}$ , suggesting that the simulation is sufficiently long.

## IV. RESULTS AND DISCUSSION

### A. The infinite periodic bundle

Figure 2 shows the density profile  $\rho(r)$  of the centers of mass of nitrogen molecules adsorbed on the infinite periodic bundle at 77 K, where  $r$  is the radial distance from the center of the bundle. Here  $\rho(r)$  is defined as the number of molecules in an infinitesimal volume

$$\rho(r) = \delta N / (2\pi r \delta r z), \quad (7)$$

where  $z$  is the tube length. The insets are the snapshots of the centers of mass of nitrogen molecules generated by accumulating 50 equilibrium configurations. At a low pressure ( $10^{-5}$  kPa) nitrogen molecules adsorb at the most favorable internal annuli, indicated by a peak at 3.4 Å in the density profile, and no molecules are present between 0 and 3.4 Å. The density increases with increasing pressure, and at a moderate pressure ( $10^{-3}$  kPa) nitrogen molecules also adsorb at the nanotube centers, indicated by a small peak at zero in the density profile. Adsorption approaches saturation at 1 kPa in the layers at both the annuli and the nanotube centers. However, layer formation is not sequential in that the second layer at the nanotube centers forms before the first layer at the annuli is saturated, and from the snapshot, we see that the adsorption behavior in each nanotube on the periodic bundle is identical. Also, no nitrogen molecule is observed to occupy the interstitial channels, consistent with the experimental observations for neon, xenon, and methane adsorption on closed-end SWNT bundles.<sup>35–38</sup> The interstitial channels may be accessible by increasing the van der Waals gap between the nanotubes or decreasing the size of the adsorbate molecule.

Figure 3(a) shows the nitrogen adsorption isotherms on the periodic bundle at the two bulk subcritical temperatures of 77 and 100 K. The points are simulation data and the lines are drawn for visual clarity. The dotted lines indicate the saturation pressures estimated from separate  $NVT$  GEMC simulations of bulk nitrogen, corresponding to 104 kPa at 77 K and 771 kPa at 100 K, which are close to the experimental

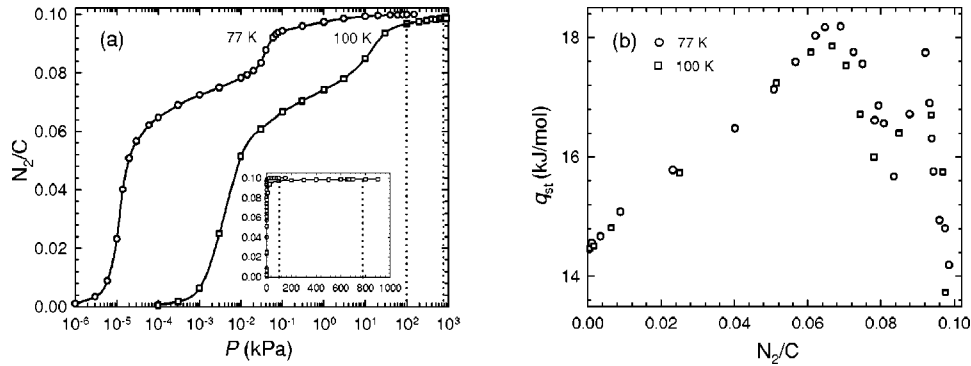


FIG. 3. (a) Nitrogen adsorption isotherms on a semilogarithmic scale of bulk pressure on the periodic bundle at 77 and 100 K. The points are simulation data, the solid lines are drawn for visual clarity, and the dotted lines indicate the bulk saturation pressures. The inset shows the isotherms on a linear scale of bulk pressure. (b) Isosteric heats of nitrogen adsorption on the periodic bundle at 77 and 100 K. Two maxima occur at  $N_2/C$  of 0.07 and 0.09, respectively.

values of 101 kPa at 77 K and 779 kPa at 100 K.<sup>43</sup> On a semilogarithmic scale of bulk pressure, two steps in the isotherms occur at  $N_2/C$  coverages of about 0.08 and 0.10, respectively, corresponding to adsorption at the two favorable sites shown in Fig. 2. At low pressures the first layer forms rapidly with increasing pressure as a result of micropore filling, whereas at moderate pressures the second layer forms gradually with increasing pressure, and at high pressures the adsorption saturates and reaches a plateau even when the bulk pressure exceeds the saturation pressure. The layer formation at 77 K is more pronounced than at 100 K due to decreased thermal motion, and occurs at a lower pressure. From zero coverage to the formation of the first layer, and then to the formation of the second layer, the transition is continuous, i.e., no steep jump, suggesting that the temperature is above the critical temperature for layer transition. On a linear scale of bulk pressure shown in the inset, the adsorption isotherms appear to be of IUPAC type I (Langmuirian), which is characteristic of a highly microporous adsorbent with pores of molecular dimensions (i.e., below 2 nm).<sup>56</sup>

Figure 3(b) shows the isosteric heats  $q_{st}$  of nitrogen adsorption on the periodic bundle at 77 and 100 K. Note that the enthalpy of bulk nitrogen  $H_B$  used in Eq. (2) to evaluate the heat of adsorption is approximated by  $R_g T$  at these conditions. There are two maxima in  $q_{st}$  at coverages close to saturation of the adsorption layers. Initially,  $q_{st}$  increases with increasing coverage during the formation of the first layer due to the cooperative attractive interaction between the admolecules. When the first layer approaches saturation at a coverage  $N_2/C$  of about 0.07,  $q_{st}$  reaches a first maximum. With further increases in pressure, additional admolecules must occupy the less favorable adsorption sites leading to a weaker adsorbate-adsorbent interaction, which results in a decrease in  $q_{st}$ . Similar behavior was observed in our previous simulations of gas adsorption on the  $C_{168}$  schwarzite.<sup>52,53</sup> As the second layer forms,  $q_{st}$  again increases, reaches the second maximum at a coverage  $N_2/C$  of about 0.09, and then decreases rapidly. Because of the limited space available, additional admolecules result in a less attractive adsorbate-adsorbate interaction and a weaker adsorbate-adsorbent interaction. The values of  $q_{st}$  at 77 and 100 K show only a small temperature dependence, and the

limiting value of  $q_{st}$  at zero coverage is approximately 14.5 kJ/mol, in accordance with 14.64 kJ/mol calculated by the test particle method.<sup>57</sup>

Figure 4 shows the density profile  $\rho(r)$  of the centers of mass of nitrogen molecules on the periodic bundle at a bulk supercritical temperature of 300 K, with the insets showing snapshots of the locations of the molecules. At a low pressure ( $10^2$  kPa), nitrogen molecules appear dispersed primarily at the annuli and at the centers inside the nanotubes. The dispersion in the distribution of the molecules increases at a moderate pressure ( $10^4$  kPa), with nitrogen molecules present throughout all locations between 0 and 3.4 Å, which is quite different from the behavior at 77 K in Fig. 2. Because of the increased thermal motion, the adsorbate molecules sample more possible adsorption sites at 300 K. However, at very high pressures ( $10^6$  kPa) distinct adsorption layers appear, and the interstitial channels become accessible to nitrogen molecules, as shown by a peak at 9.7 Å in the density profile. Since the interstitial channel is narrow, nitrogen molecules therein are preferentially aligned with their bonds parallel to the nanotube axis. (There are 12 663 and 31 121 centers of mass in the snapshots at  $10^4$  and  $10^6$  kPa, respectively, although the former may appear to contain more than the latter.) Similar to the behavior at 77 K, the layer formation is not sequential, but it is less pronounced here, also due to stronger thermal motion.

Figure 5(a) shows the nitrogen adsorption isotherm on the periodic bundle at 300 K. On a semilogarithmic scale of bulk

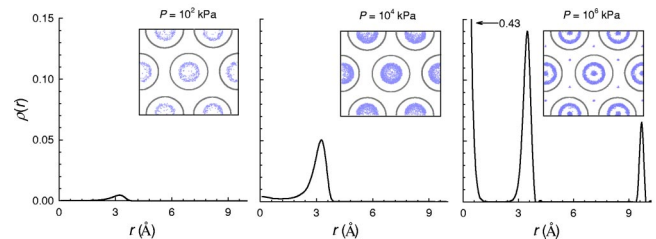


FIG. 4. (Color online) Density profiles of the centers of mass of nitrogen molecules versus the distance from the center of the periodic bundle at 300 K. The insets are snapshots generated by accumulating 50 equilibrium configurations.

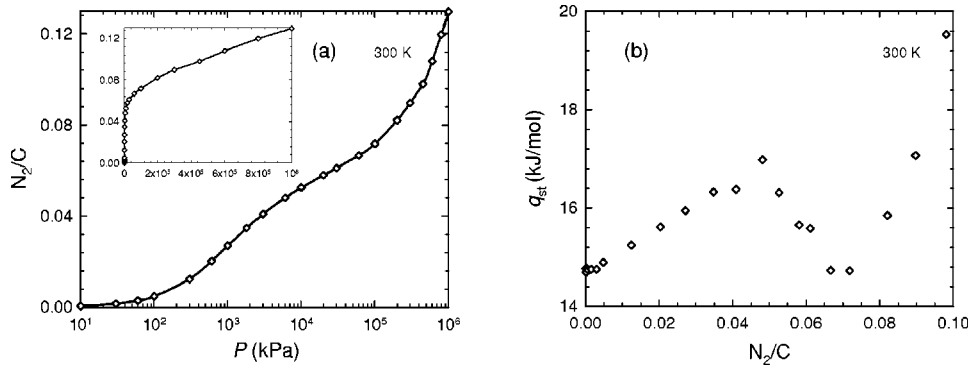


FIG. 5. (a) Nitrogen adsorption isotherm on a semilogarithmic scale of bulk pressure on the periodic bundle at 300 K. The points are simulation data and the solid line is drawn for visual clarity. The inset shows isotherm on a linear scale of bulk pressure. (b) Isothermic heat of nitrogen adsorption on the periodic bundle at 300 K. A maximum occurs at  $N_2/C$  of 0.05.

pressure, the formation of one layer is barely seen at a coverage  $N_2/C$  of about 0.06, and in general the isotherm has a rounded shape. Similar to the subcritical adsorption at 77 and 100 K of Fig. 3(a), the isotherm shown in the inset is also of type I. This type of isotherm is not surprising, since generally, an adsorbate above its critical temperature does not form multiple layers. As expected, at any given pressure the coverage at 300 K is much lower than at 77 and 100 K, as adsorption is an exothermic process so that increasing temperature reduces adsorption capacity.

Figure 5(b) shows the isosteric heat  $q_{st}$  of nitrogen adsorption on the periodic bundle at 300 K. Unlike Fig. 3(b) at subcritical temperatures; here only a single maximum exists at a coverage  $N_2/C$  of about 0.05 corresponding to the formation of a single adsorbed layer seen in the isotherm of Fig. 5(a). Above 0.07,  $q_{st}$  continues increasing. This increase is not a result of strong gas-surface or gas-gas attractions; instead it is due to the large value of  $H_B$  in Eq. (2) used to evaluate  $q_{st}$  at high pressures. At this condition, nitrogen is not an ideal gas and  $H_B$  cannot be approximated by  $R_g T$ . The limiting value of  $q_{st}$  at zero coverage is approximately 14.8 kJ/mol, slightly larger than that at the subcritical temperature of Fig. 3(b), and consistent with 14.86 kJ/mol calculated by the test particle method.<sup>57</sup>

**B. The finite isolated bundle**

Figure 6 shows the density profiles  $\rho(r)$  of the centers of mass of nitrogen molecules on the finite isolated bundle at 77 K, where  $r$  is the radial distance from the center of the bundle. At a low pressure ( $10^{-5}$  kPa), nitrogen molecules adsorb at the grooves between adjacent nanotubes and in annuli within the nanotubes. Since the groove region is very

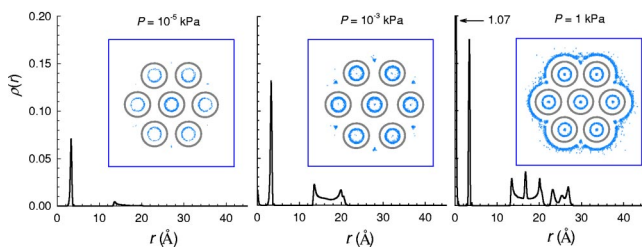


FIG. 6. (Color online) Density profiles of the centers of mass of nitrogen molecules versus the distance from the center of the isolated bundle at 77 K. The insets are snapshots generated by accumulating 50 equilibrium configurations.

small, it can be occupied only by a few molecules. As a result of the higher adsorption energy, the density at the annulus in the middle nanotube is higher than in the neighboring nanotubes. Moreover, the adsorbate density in the annulus of the neighboring nanotube is not uniform, in that the density is greater adjacent to the middle nanotube than adjacent to the external surface. At a moderate pressure ( $10^{-3}$  kPa) nitrogen molecules adsorb at the ridges surrounding the nanotubes and at the nanotube centers. At higher pressure (1 kPa) and increased coverage, adsorption occurs on the external surface near the ridges. At still higher pressures close to saturation (not shown), multiple adsorption layers form on the external surface away from the ridges. The density profiles show that the layer formation is not sequential.

Figure 7(a) shows the nitrogen adsorption isotherms on the isolated bundle at two bulk subcritical temperatures of 77 and 100 K, and the dotted lines are the saturation vapor pressures of bulk nitrogen estimated from  $NVT$  GEMC simulations. Unlike on the infinite periodic bundle, the adsorption isotherm indicates multilayer formation, with the first layer occurring at a coverage  $N_2/C$  of 0.08, the second layer at 0.18, and eventually multilayer adsorption (wetting) on the external surface as the saturation condition of bulk nitrogen is approached. The first layer corresponds to adsorption in the annuli and the grooves, and the second layer at the ridges and the nanotube centers, and the layer formation is continuous. There is significant adsorption on the external surface of the isolated bundle, and the extent of adsorption, that is, the coverage  $N_2/C$  is larger than on the infinite periodic bundle, especially approaching the bulk saturation pressure. The isotherm is of type II as shown on a linear scale of bulk pressure in the inset, which is the signature of adsorption in a macroporous adsorbent, or on the surface of a non-porous adsorbent that allows multilayer formation.<sup>56</sup>

Qualitatively, our results support the observation of the type II isotherm found from measurements of gas adsorption in SWNT bundles at subcritical temperatures.<sup>5-7</sup> However, obtaining quantitative agreement between simulation and experiment is difficult for several reasons. First, the real nanotubes on which measurements have been made are not pure, vary in diameter and structure (chirality), and frequently contain metallic catalyst residues and amorphous carbon particles. Second, nanotubes may be single ended or closed ended rather than open ended, and hence the interiors may be inaccessible or only partially accessible by adsorbate mol-

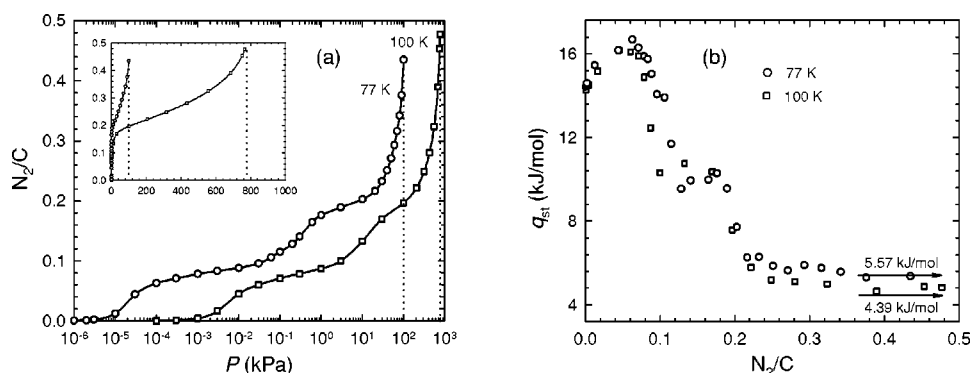


FIG. 7. (a) Nitrogen adsorption isotherms on a semilogarithmic scale of bulk pressure on the isolated bundle at 77 and 100 K. The points are simulation data, the solid lines are drawn for visual clarity, and the dotted lines indicate the bulk saturation pressures. The inset shows isotherms on a linear scale of bulk pressure. (b) Isothermic heats of nitrogen adsorption on the isolated bundle at 77 and 100 K. Two maxima occur at  $N_2/C$  of 0.06 and 0.17, respectively. The horizontal arrows indicate the vaporization enthalpies of bulk nitrogen at these two temperatures.

ecules. Third, there can be defect sites containing oxygenated groups that may block the entrance of adsorbate into nanotubes, and thus lower adsorption capacity.<sup>58</sup> Finally, the nanotube-nitrogen interaction has been assumed to be the same as the graphite-nitrogen interaction, which may be inaccurate.

Figure 7(b) shows the isothermic heats  $q_{st}$  of nitrogen adsorption on the isolated bundle at 77 and 100 K. The low-pressure portion of the curve resembles those on the periodic bundle of Fig. 3(b), i.e., two maxima exist at coverages close to the saturation of the two individual layers. Initially,  $q_{st}$  increases with increasing coverage during the formation of the first layer due to the cooperative interaction between the admolecules. When the first layer approaches a coverage  $N_2/C$  of about 0.06,  $q_{st}$  achieves the first maximum. Then with increased coverage, the admolecules occupy less favorable adsorption sites leading to a weaker adsorbate-adsorbent interaction, which results in a decrease in  $q_{st}$ . At the start of the formation of the second layer  $q_{st}$  again increases, reaches the second maximum at a coverage  $N_2/C$  of about 0.17, and then decreases. Multiple adsorbed layers form as the bulk pressure is further increased, and finally wetting occurs as the bulk saturation pressure is approached. At this condition,  $q_{st}$  is close to the vaporization enthalpy of bulk nitrogen, for example, 5.57 kJ/mol at 77 K,<sup>59</sup> and 4.39 kJ/mol at 100 K,<sup>60</sup> as indicated by the two horizontal arrows. Similar behavior for the heat of adsorption has been observed experimentally for krypton and ethane adsorption on graphitized thermal carbon black.<sup>61</sup> Furthermore, when wetting occurs, the density of the adsorbate far from the adsorbent is nearly that of the saturated liquid, 28.71 mol/l at 77K, and 24.60 mol/l at 100 K.<sup>59</sup> This is because these additional, faraway admolecules are in a bulklike environment in which they interact almost exclusively with other adsorbate molecules. As in Fig. 3(b), there is a small temperature dependence of  $q_{st}$  at 77 and 100 K, and the limiting value at zero coverage is about 14.3 kJ/mol.

Figure 8 shows the density profile  $\rho(r)$  of the centers of mass of nitrogen molecules on the isolated bundle at 300 K, with the insets showing the snapshots. At a pressure of  $10^3$  kPa nitrogen molecules are inside the nanotubes and in

the bulk region. The densities in both regions increase as pressure increases to  $10^4$  and  $10^5$  kPa, with the larger density change in the bulk region. Due to the increased thermal motion, nitrogen molecules are not in an ordered structure within the nanotube. However, unlike on the infinite nanotube bundle, nitrogen molecules do not intercalate the interstitial channels at the highest pressure considered here as the bulk region is energetically more favorable. As mentioned earlier, not all the molecules in the simulation cell of the isolated bundle are admolecules, and we need to correct for this in determining the extent of coverage. From the density profile, the density approaches the bulk value at a distance of about 40 Å, so that we consider only molecules within this cutoff distance to be adsorbed. This correction is negligible at low pressures of Fig. 6, where there are few nitrogen molecules beyond the cutoff distance; however, it is significant at high pressures.

Figure 9(a) shows the nitrogen adsorption isotherm calculated in this way on the isolated bundle at 300 K. On a semilogarithmic scale of bulk pressure, the isotherm does not show layer formation. On a linear scale, the isotherm appears to be of type I, as expected.

Figure 9(b) shows the isothermic heat  $q_{st}$  of nitrogen adsorption on the isolated bundle at 300 K. Here no maximum exists, and above a coverage  $N_2/C$  of 0.2,  $q_{st}$  continues increasing with increasing coverage. As before, this is not due to strong gas-surface or gas-gas interactions, but is a result of the large value of the enthalpy of bulk nitrogen at high pres-

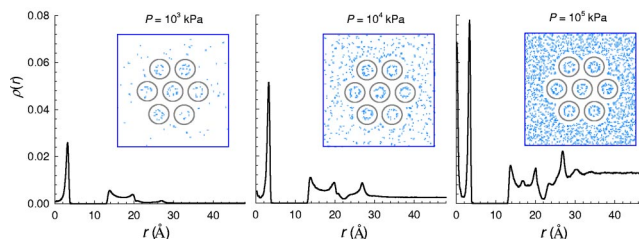


FIG. 8. (Color online) Density profiles of the centers of mass of nitrogen molecules versus the distance from the center of the isolated bundle at 300 K. The insets are snapshots generated by accumulating 50 equilibrium configurations.

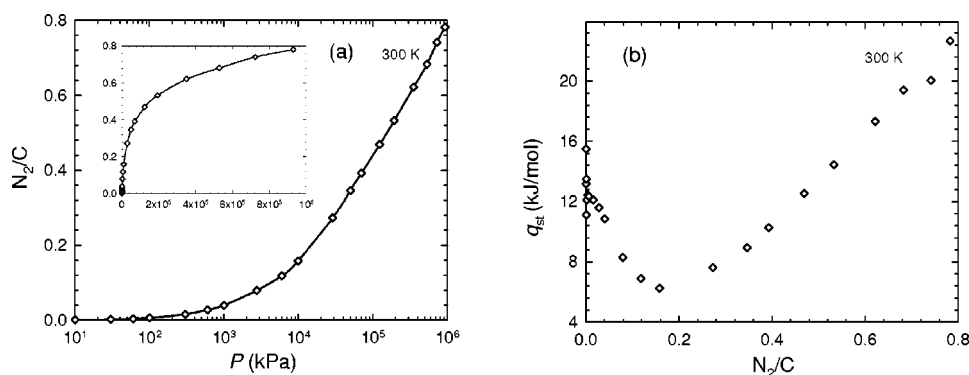


FIG. 9. (a) Nitrogen adsorption isotherm on a semilogarithmic scale of bulk pressure on the isolated bundle at 300 K. The points are simulation data and the solid line is drawn for visual clarity. The inset shows the isotherm on a linear scale of bulk pressure. (b) Isothermic heat of nitrogen adsorption on the isolated bundle at 300 K. No maximum occurs.

tures. The limiting value of  $q_{st}$  at zero coverage is estimated to be 12.8 kJ/mol, lower than that at the subcritical temperatures of Fig. 7(b).

## V. CONCLUSIONS

This work reveals the significant role of the external surface of the nanotube bundle in gas physisorption. On the infinite periodic bundle with no external surface, adsorption is of type I at both subcritical and supercritical temperatures, and adsorption occurs inside the nanotubes, first at the annuli and then at the tube centers. The interstitial channels become accessible to nitrogen molecules only at high pressures. In contrast, as a result of the external surface on the finite isolated bundle, the adsorption is of type II at subcritical temperatures, as has been observed in experiments. Adsorption occurs first at the annuli inside the nanotubes and at the grooves between the nanotubes, at higher pressures also at the ridges surrounding nanotubes and at the nanotube centers, and at still higher pressures on the external surface. The formation of external multilayer leads to wetting as the bulk phase approaches saturation. No adsorption occurs at the interstitial channels. When temperature increases from subcritical to supercritical of the bulk adsorbate, the adsorption on the finite isolated bundle changes from type II to type I. The results provide a rational physical elucidation for the difference between experimental observation and previous theoretical prediction.

The empirical potential for gas adsorption on graphite has been used for the interaction between the gas and the nanotube. This may be reasonable as a nanotube may be regarded approximately as a curved graphene sheet. However, it is likely that the site-site interaction potential is influenced by the curvature of the carbon surface. The curvature of the graphene sheet should increase the localization of the electron density, causing a shift of the hybridization of carbon atoms from purely  $sp^2$  to somewhat  $sp^3$ . The electronic band structure of carbon nanotube has been found to be sensitive to the type and curvature of nanotube.<sup>62</sup> Consequently, the site-site interaction potentials may depend on the local bonding structure of the carbon. In fact, recent experiments have determined that the low-coverage binding energies of methane, xenon, and oxygen on nanotube bundles are 76%, 74%, and 55%, respectively, larger than on planar graphite.<sup>63–65</sup> Therefore, improvement of the interaction potentials accounting for curvature and bonding is needed to more accurately investigate gas adsorption on nanotubes.

## ACKNOWLEDGMENTS

We acknowledge the support of the National Science Foundation under Grant No. EEC-0085461 and the Department of Energy under Grant No. DE-FG02-85ER13436. It is a pleasure to thank Patrick Bernier (Université de Montpellier II) and Akihiko Fujiwara (Japan Advanced Institute of Science and Technology) for helpful communications.

\*Corresponding author. Electronic address: jiangj@che.udel.edu

<sup>1</sup>S. Iijima, *Nature (London)* **354**, 56 (1991).

<sup>2</sup>S. Iijima, *Physica B* **323**, 1 (2002).

<sup>3</sup>P. M. Ajayan, *Chem. Rev. (Washington, D.C.)* **99**, 1787 (1999).

<sup>4</sup>H. J. Dai, *Acc. Chem. Res.* **35**, 1035 (2002).

<sup>5</sup>A. Fujiwara, K. Ishii, H. Suematsu, H. Kataura, Y. Maniwa, S. Suzuki, and Y. Achiba, *Chem. Phys. Lett.* **336**, 205 (2001).

<sup>6</sup>M. Muris, N. Dufau, M. Bienfait, N. D. Pavlovsky, Y. Grillet, and J. P. Palmari, *Langmuir* **16**, 7019 (2000).

<sup>7</sup>D. H. Yoo, G. H. Rue, Y. H. Hwang, and H. K. Kim, *J. Phys. Chem. B* **106**, 3371 (2002).

<sup>8</sup>D. H. Yoo, G. H. Rue, M. H. W. Chan, Y. H. Hwang, and H. K. Kim, *J. Phys. Chem. B* **107**, 1540 (2003).

<sup>9</sup>S. Inoue, N. Ichikuni, T. Suzuki, T. Uematsu, and K. Kaneko, *J. Phys. Chem. B* **102**, 4689 (1998).

<sup>10</sup>E. B. Mackie, R. A. Wolfson, L. M. Arnold, K. Lafdi, and A. D. Migone, *Langmuir* **13**, 7197 (1997).

<sup>11</sup>J. Hilding, E. A. Grulke, S. B. Sinnott, D. Qian, R. Andrews, and M. Jagtoyen, *Langmuir* **17**, 7540 (2001).

<sup>12</sup>A. C. Dillon and M. J. Heben, *Appl. Phys. A: Mater. Sci. Process.* **72**, 133 (2001).

<sup>13</sup>R. G. Ding, G. Q. Lu, Z. F. Yan, and M. A. Wilson, *J. Nanosci. Nanotechnol.* **1**, 7 (2001).

<sup>14</sup>H. M. Cheng, Q. H. Yang, and C. Liu, *Carbon* **39**, 1447 (2001).

<sup>15</sup>F. L. Darkrim, P. Malbrunot, and G. P. Tartaglia, *Int. J. Hydrogen Energy* **27**, 193 (2002).

<sup>16</sup>A. Zuttel, P. Sudan, P. Mauron, T. Kiyobayashi, C. Emmenegger, and L. Schlapbach, *Int. J. Hydrogen Energy* **27**, 203 (2002).

<sup>17</sup>Y. F. Yin, T. Mays, and B. McEnaney, *Langmuir* **15**, 8714 (1999).

<sup>18</sup>X. Zhang and W. Wang, *Fluid Phase Equilib.* **194–197**, 289 (2002).

- <sup>19</sup>X. Zhang and W. Wang, *Phys. Chem. Chem. Phys.* **4**, 3048 (2003).
- <sup>20</sup>Q. Y. Wang and J. K. Johnson, *J. Phys. Chem. B* **103**, 4809 (1999).
- <sup>21</sup>F. Darkrim and D. Levesque, *J. Phys. Chem. B* **104**, 6773 (2000).
- <sup>22</sup>F. Darkrim and D. Levesque, *J. Chem. Phys.* **109**, 4981 (1998).
- <sup>23</sup>F. Darkrim, A. Aoufi, and D. Levesque, *Mol. Simul.* **24**, 51 (2000).
- <sup>24</sup>C. Gu, G. H. Gao, Y. X. Yu, and T. Nitta, *Fluid Phase Equilib.* **194–197**, 297 (2002).
- <sup>25</sup>D. Levesque, A. Gicquel, F. L. Darkrim, and S. B. Kayiran, *J. Phys.: Condens. Matter* **14**, 9285 (2002).
- <sup>26</sup>Y. F. Yin, T. Mays, and B. McEnaney, *Langmuir* **16**, 10521 (2000).
- <sup>27</sup>V. V. Simonyan, P. Diep, and J. K. Johnson, *J. Chem. Phys.* **111**, 9778 (1999).
- <sup>28</sup>V. V. Simonyan, J. K. Johnson, A. Kuznetsova, and J. T. Yates, *J. Chem. Phys.* **114**, 4180 (2001).
- <sup>29</sup>M. R. Smith, E. W. Bittner, W. Shi, J. K. Johnson, and B. C. Bockrath, *J. Phys. Chem. B* **107**, 3752 (2003).
- <sup>30</sup>Q. Y. Wang and J. K. Johnson, *J. Chem. Phys.* **110**, 577 (1999).
- <sup>31</sup>H. S. Cheng, G. P. Pez, and A. C. Cooper, *J. Am. Chem. Soc.* **123**, 5845 (2001).
- <sup>32</sup>J. J. Zhao, A. Buldum, J. Han, and J. P. Lu, *Nanotechnology* **13**, 195 (2002).
- <sup>33</sup>A. Thess, R. Lee, P. Nikolaev, H. J. Dai, P. Petit, J. Robert, C. H. Xu, Y. H. Lee, S. G. Kim, A. G. Rinzler, D. T. Colbert, G. E. Scuseria, D. Tomanek, J. E. Fischer, and R. E. Smalley, *Science* **273**, 483 (1996).
- <sup>34</sup>C. Journet, W. K. Maser, P. Bernier, A. Loiseau, M. L. delaChapelle, S. Lefrant, P. Deniard, R. Lee, and J. E. Fischer, *Nature (London)* **388**, 756 (1997).
- <sup>35</sup>S. Talapatra, A. Z. Zambano, S. E. Weber, and A. D. Migone, *Phys. Rev. Lett.* **85**, 138 (2000).
- <sup>36</sup>S. Talapatra and A. D. Migone, *Phys. Rev. Lett.* **87**, 206106 (2001).
- <sup>37</sup>S. Talapatra, V. Krungleviciute, and A. D. Migone, *Phys. Rev. Lett.* **89**, 246106 (2002).
- <sup>38</sup>J. C. Lasjaunias, K. Biljakovic, J. L. Sauvajol, and P. Monceau, *Phys. Rev. Lett.* **91**, 025901 (2003).
- <sup>39</sup>K. A. Williams and P. C. Eklund, *Chem. Phys. Lett.* **320**, 352 (2000).
- <sup>40</sup>S. M. Gatica, M. J. Bojan, G. Stan, and M. W. Cole, *J. Chem. Phys.* **114**, 3765 (2001).
- <sup>41</sup>M. M. Calbi, S. M. Gatica, M. J. Bojan, and M. W. Cole, *J. Chem. Phys.* **115**, 9975 (2001).
- <sup>42</sup>M. M. Calbi and M. W. Cole, *Phys. Rev. B* **66**, 115413 (2002).
- <sup>43</sup>D. R. Lide, *CRC Handbook of Chemistry and Physics* (CRC Press, Boca Raton, FL, 1991).
- <sup>44</sup>C. S. Murthy, K. Sing, M. L. Klein, and I. R. McDonald, *Mol. Phys.* **41**, 1387 (1980).
- <sup>45</sup>M. J. Bojan and W. A. Steele, *Langmuir* **3**, 116 (1987); **3**, 1123 (1987).
- <sup>46</sup>O. Ikkala and G. T. Brinke, *Science* **295**, 2407 (2002).
- <sup>47</sup>D. Nicholson and N. G. Parasonage, *Computer Simulation and The Statistical Mechanics of Adsorption* (Academic Press, New York, 1982).
- <sup>48</sup>A. Z. Panagiotopoulos, N. Quirke, M. Stapleton, and D. J. Tildesley, *Mol. Phys.* **63**, 527 (1988).
- <sup>49</sup>A. Z. Panagiotopoulos, *Mol. Phys.* **61**, 813 (1987).
- <sup>50</sup>A. Z. Panagiotopoulos, *Mol. Phys.* **62**, 701 (1987).
- <sup>51</sup>S. C. McGrother and K. E. Gubbins, *Mol. Phys.* **97**, 955 (1999).
- <sup>52</sup>J. W. Jiang, J. B. Klauda, and S. I. Sandler, *Langmuir* **19**, 3512 (2003).
- <sup>53</sup>J. W. Jiang and S. I. Sandler, *Langmuir* **19**, 5936 (2003).
- <sup>54</sup>T. Vuong and P. A. Monson, *Langmuir* **12**, 5425 (1996).
- <sup>55</sup>D. Frenkel and B. Smit, *Understanding Molecular Simulation* (Academic Press, San Diego, 1996).
- <sup>56</sup>F. Rouquerol, J. Rouquerol, and K. Sing, *Adsorption: By Powders and Porous Solids* (Academic Press, London, 1999).
- <sup>57</sup>J. W. Jiang, N. J. Wagner, and S. I. Sandler (unpublished).
- <sup>58</sup>J. C. Charlier, *Acc. Chem. Res.* **35**, 1063 (2002).
- <sup>59</sup>*NIST Chemistry WebBook*, NIST Standard Reference Database No. 69, edited by P. J. Linstrom and W. G. Mallard (National Institute of Standards and Technology, Gaithersburg, MD, 2003).
- <sup>60</sup>The vaporization enthalpy of bulk nitrogen at 100 K is estimated from the Watson relation  $H_2^{\text{vap}} = H_1^{\text{vap}} [(T_c - T_2)/(T_c - T_1)]^{0.375}$ , where  $T_c$  is the critical temperature.
- <sup>61</sup>N. N. Avgul and A. V. Kiselev, in *Chemistry and Physics of Carbon*, edited by P. L. Walker (Marcel Dekker, New York, 1970), Vol. 6.
- <sup>62</sup>M. K. Kostov, H. Cheng, A. C. Cooper, and G. P. Pez, *Phys. Rev. Lett.* **89**, 146105 (2002).
- <sup>63</sup>S. E. Weber, S. Talapatra, C. Journet, Z. Zambano, and A. D. Migone, *Phys. Rev. B* **61**, 13 150 (2000).
- <sup>64</sup>A. J. Zambano, S. Talapatra, and A. D. Migone, *Phys. Rev. B* **64**, 075415 (2001).
- <sup>65</sup>H. Ulbricht, G. Moos, and T. Hertel, *Phys. Rev. B* **66**, 075404 (2002).